

# A new 3D cupric coordination polymer as chemiresistor humidity sensor: narrow hysteresis, high sensitivity, fast response and recovery

Xiao-Jing Lv<sup>1,2</sup>, Ming-Shui Yao<sup>1</sup>, Guan-E Wang<sup>1</sup>, Yan-Zhou Li<sup>1,2</sup> & Gang Xu<sup>1\*</sup><sup>1</sup>State Key Laboratory of Structural Chemistry, Fujian Institute of Research on the Structure of Matter, Chinese Academy of Sciences, Fuzhou 350002, China<sup>2</sup>University of Chinese Academy of Sciences, Chinese Academy of Sciences, Beijing 100039, China

Received April 1, 2017; accepted May 8, 2017; published online July 18, 2017

A new three-dimensional coordination polymer composed of  $\text{Cu}^{2+}$  centres and semiquinoid linkers ( $\text{d}(\text{hbq})^{2-}$ ) was synthesized which was composed by two independent, enantiomeric, interpenetrated  $[\text{Cu}_2(\text{d}(\text{hbq})_3)]^{2-}$  networks with (10,3)-a topology. The compound has good water stability and typical behaviors of semiconductor, whose conductivity increases along with raising temperature. The chemiresistive humidity sensor made from this material shows good properties including linear sensitivity, high response, fast response and recovery, and particularly narrow hysteresis during humidity adsorption and desorption.

**coordination polymer, chemiresistive humidity sensor, narrow hysteresis, fast response & recovery**

**Citation:** Lv XJ, Yao MS, Wang GE, Li YZ, Xu G. A new 3D cupric coordination polymer as chemiresistor humidity sensor: narrow hysteresis, high sensitivity, fast response and recovery. *Sci China Chem*, 2017, 60: 1197–1204, doi: 10.1007/s11426-017-9079-5

## 1 Introduction

Chemiresistive sensor devices are becoming increasingly important, due to their simplicity, low power consumption, modularity, broad applicability and ease of integration with standard electronics. These advantages open up their wide applications in wearable devices, intelligent automobile, smart electrical home appliances, and environmental and food quality control [1,2]. For the last few decades, various materials have been developed for chemiresistive gas/humidity sensors, such as metal oxide semiconductors [3], conductive polymers [4], carbon based materials (such as carbon nanotube [5], graphene [6]).

Coordination polymers (CPs) are coordination compounds containing identical metal complex fragments (central atoms

surrounded by ligands), which repeat in one, two, or three dimensions [7]. CPs have been intensively studied and introduced to a myriad of applications, including gas separation and storage, luminescence, catalysis, etc. [8,9]. Increased attention has also been paid to develop CPs as next-generation sensing materials owing to their specific features, such as structure diversity and designability, tunable sensing active sites, large surface area and extraordinary adsorption affinities [10]. Various CPs-based electrical sensors have been developed towards gas molecules, humidity and so on. For example, CPs with 7,7,8,8-tetracyanoquinodimethane (TCNQ) and 2,3,5,6-tetrafluoro-7,7,8,8-tetracyanoquinodimethane (TCNQF<sub>4</sub>) as ligands have been studied for chemiresistive sensor by O'Mullane's group [11,12], where these CPs showed a response to  $\text{NO}_2$  and  $\text{NH}_3$  gases at 25 °C. A zeolitic imidazolate framework, ZIF-67, was employed by Zhang's group [13] as a promising formaldehyde gas sensor at a medium operating temperature (150 °C). Lang

\*Corresponding author (email: gxu@fjirsm.ac.cn)

and co-workers [14] used 1D silver(I)-bromide-thiol coordination polymer as the sensor for detecting ammonia and amines in water. Dincă *et al.* [15,16] demonstrated that a chemiresistive sensor array containing three isostructural porous CPs can reliably distinguish five categories of volatile organic compounds. Nanorods of conductive porous CP, Cu<sub>3</sub>HHTP<sub>2</sub>, reported by Mirica's group [17] were *in situ* grown on shrinkable polymer films for detecting ppm-level NH<sub>3</sub>, NO, and H<sub>2</sub>S. CPs have shown great promising as the key materials of chemiresistor sensor. However, designing and synthesising of CPs that can be applied in sensor with fast responsibility, high sensitivity, good stability is still a great challenge.

Humidity is one of the most commonly measured physical quantities, because it is an inevitable constituent in the air due to abundant water in our environment and it changes largely with season, temperature, location, etc. [18]. Thus, high performance humidity sensors are indispensable in diverse humidity-sensitive fields including agriculture, grain preservation, industrial process and human life [18,19]. At present, there are three types of CP-based electrical sensors: capacitive type, alternative current (AC) impedance type and direct current (DC) resistance type. Most CP-based humidity sensors are capacitive type due to low power consumption and high output signals [18,20,21]. Our previous work has demonstrated that a capacitive humidity sensor based on the Cu<sub>3</sub>TCP nano-flake showed good capacitance response within the humidity range of 60%–98% relative humidity (RH) [22]. However, hysteresis is a common problem virtually for all kinds of capacitive humidity sensors due to the slower diffusion time of moisture sensitive films while dehumidifying, which is often a serious drawback because of the corresponding unreliable responses [21]. Another type of CP-based humidity resistive sensor is mainly based on detecting the signal of impedance change in AC filed [23,24]. This type of sensors exhibited good long-term stability and high sensitivity. However, the application of them is hampered by broad hysteresis and fair response-recovery [25]. Compared with AC type, DC sensors show advantages of real-time monitoring, high sensitivity and the potential to be integrated into low-cost devices, narrow hysteresis and fast response-recovery [26].

In this work, we report the synthesis and detailed single crystal structure of a 3D CP, (NBu<sub>4</sub>)<sub>2</sub>Cu<sub>2</sub>(d**hbq**)<sub>3</sub> (**1**), as well as its application in humidity chemiresistive sensor as active material. Compound **1** was synthesized with Cu<sup>2+</sup> and redox active d**hbq**<sup>2-</sup>, which shows good water-stable and typical semiconductive behavior. The DC chemiresistor sensor of compound **1** shows excellent humidity sensing properties with linear sensitivity in a broad relative humidity range, high response of a 10<sup>4</sup> times enhanced conductivity under 80% RH, fast response and recovery, and narrow hysteresis during humidity adsorption and desorption.

## 2 Experimental

### 2.1 Materials

All reagents were purchased commercially and used without further purification. Tetrabutylammonium iodide (NBu<sub>4</sub>I), 2,5-dihydroxybenzoquinone and Cu(Ac)<sub>2</sub> were purchased from Aladdin (USA). *N,N*-diethylformamide (DMF) was purchased from Sinopharm Group Co., Ltd. (China). Water was purified using the Milli-Q purification system. Sensor substrates (13.5 mm×7 mm, 0.5 mm in thickness) with five pairs of Ag-Pd interdigitated electrodes (both the width and distance were 200 μm) were purchased from Beijing Elite Tech Co. (China).

### 2.2 Synthesis of compound 1 single crystals

2,5-Dihydroxybenzoquinone (35 mg, 0.25 mmol) and an excess of NBu<sub>4</sub>I (400 mg) were dissolved in 10 mL DMF solution. Then, the above solution was carefully added to an aqueous solution (10 mL) containing Cu(Ac)<sub>2</sub>·6H<sub>2</sub>O (70 mg, 0.37 mmol). The mixture was stirred and dropped with concentrated NaOH to adjust pH≈10. Then it was capped and allowed to stand at room temperature. Red block-like single crystals began to form in a week. One of these crystals was used for X-ray crystallography. Elemental analysis calcd.: C, 58.82%; H, 7.05%; N, 2.74%. Found: C, 55.25%; H, 7.25%; N, 2.59%.

### 2.3 Powder X-ray diffraction and single crystal structure determination

Powder X-ray diffraction was performed on Rigaku Mini-Flex II diffractometer (Japan) using Cu Kα radiation by keeping the powdered sample on a silicon substrate. The diffraction patterns were collected in the 2θ range of 5°–45° with a step size of 0.02°. Single-crystal X-ray diffraction data of compound **1** were collected on a SuperNova diffractometer (Rigaku, Japan) with the Cu Kα radiation (λ=1.5406 Å). Absorption corrections were applied by using multi-scan program. The structure was determined by direct methods and refined on F<sup>2</sup> by full-matrix least-squares method using the SHELXTL-2016 program package [27]. The X-ray diffraction crystallographic data and structure refinements for compound **1** are demonstrated in Table 1. Crystallographic data for compound **1** reported in this paper have been deposited in the Cambridge Crystallographic Data Centre with CCDC 1528501. This data can be obtained free of charge from the Cambridge Crystallographic Data Centre via [www.ccdc.cam.ac.uk/data\\_request/cif](http://www.ccdc.cam.ac.uk/data_request/cif).

### 2.4 Characterization

The Fourier transform infrared spectroscopy (FT-IR) spectra were recorded on a Bruker VERTEX70 FT-IR spectrometer

**Table 1** Crystal data and structure refinement for compound **1**

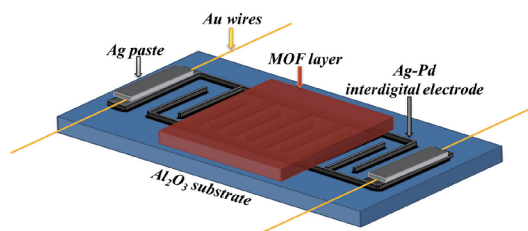
Crystal data	(NBu <sub>4</sub> ) <sub>2</sub> Cu <sub>2</sub> (dhbq) <sub>3</sub>
Empirical formula	C <sub>9</sub> H <sub>3</sub> Cu <sub>1</sub> O <sub>6</sub>
Formula weight	270.65
Temperature	100(2) K
Wavelength	1.54184 Å
Crystal system	Cubic
space group	<i>I</i> -43 <i>d</i>
Unit cell dimensions	<i>a</i> =22.1195(4) Å, $\alpha$ =90° <i>b</i> =22.1195(4) Å, $\beta$ =90° <i>c</i> =22.1195(4) Å, $\gamma$ =90°
Volume	10822.5(6) Å <sup>3</sup>
Z	16
<i>F</i> (000)	2144
Limiting indices	-27 ≤ <i>h</i> ≤ 26; -14 ≤ <i>k</i> ≤ 26; -25 ≤ <i>l</i> ≤ 27
Reflections collected/unique	15731/1720
Completeness to theta=67.684	100.0%
Data/restraints/parameters	1720/6/50
GOF on <i>F</i> <sup>2</sup>	1.057
Final <i>R</i> indices [ <i>I</i> >2σ( <i>I</i> )]	<i>R</i> <sub>1</sub> =0.0676, <i>wR</i> <sub>2</sub> =0.1776 <sup>a)</sup>
<i>R</i> indices (all data)	<i>R</i> <sub>1</sub> =0.0683, <i>wR</i> <sub>2</sub> =0.1785

$$a) R_1 = \frac{\sum |F_o| - |F_c|}{\sum |F_o|}, wR_2 = \frac{[\sum (F_o^2 - |F_c|^2) / \sum |F_o|^2]^{1/2}}{1}$$

(Germany) in 4000–400 cm<sup>-1</sup> region using KBr pellets. Thermogravimetric analyses were done on a NETZSCHSTA449C analyzer (Germany) with a heating rate of 10 °C min<sup>-1</sup> from 25 to 1200 °C, with a N<sub>2</sub> flow rate of 20 mL min<sup>-1</sup>. UV-Vis-NIR diffuse reflectance spectra were recorded on a Lambda 950 (PerkinElmer, USA) using BaSO<sub>4</sub> as a standard. The electrical measurements were performed using a Keithley 4200 (USA).

## 2.5 Sensing property test

The crystals of compound **1** were ground with ethanol to form a suspension in mortar. The size of grains is varied from nanometer to micrometer (Figure S1(a), Supporting Information online), which is common for grinding method. From the cross sectional view, the thickness of the coating film is about 5 μm (Figure S1(b)). Then, the suspension was drop-casted on an aluminium oxide substrate with Ag-Pd interdigitated electrodes to form the sensing layer. Two Au leading wires were glued onto the two electrodes by silver paste. Before measurement, the samples were degassed in vacuum at 100 °C for overnight. Figure 1 shows the structure of the humidity sensor prototype constructed on a DC circuit. The humidity sensing characterization was conducted by a home-made system reported previously [28]. The humidity response experiment was carried out by placing the sensor device in a sealed quartz chamber at room temperature and

**Figure 1** A schematic illustration of the humidity sensor prototype (color online).

monitoring the resistance of the device in different relative humidity with dry air as carried gas. The sensor device applied constant voltage (1.0 V) via a Keithley 2602B (USA) source meter and measured the current of the sensor through the exposure and recovery cycles. Humidity gas was introduced into the quartz tube via mass flow controllers. The constant flow was 600 mL min<sup>-1</sup>. All of the sensing measurements were performed at ambient temperature.

## 3 Results and discussion

### 3.1 Structural description

Single crystal X-ray diffraction analysis reveals that compound **1** crystallized in a cubic space group *I*-43*d* (Table 1), an isostructural metal organic framework (MOF) to previous report [29]. Each Cu atom adopts a slightly distorted octahedral geometry coordinated by six oxygen atoms from three separately benzoquinone rings to form a CuO<sub>6</sub> octahedron (Figure 2(b)). The CuO<sub>6</sub> octahedron then connected by 2,5-dihydroxybenzoquinone moieties to form a 3D porous structure with hexagonal channels along the [111] direction (Figure 2(c)). The O–Cu–O bond angles are 78.41°–96.92° and the Cu–O distances are 1.99 Å, which are comparable with those of carboxylate-based Cu-MOF [30]. Compound **1** contains two independent, enantiomeric (10,3)-a networks of opposite chiralities that interpenetrate in the manner shown in Figure 2(d). The charge of the network is compensated by NBu<sub>4</sub><sup>+</sup> which located in the channels is highly disordered in the networks. The pores in the structure are almost completely filled by NBu<sub>4</sub><sup>+</sup> cations.

The powder X-ray diffraction (PXRD) pattern in Figure 3(a) shows that all of the peaks are well consistent with the simulated PXRD pattern. No impurity phase was observed. FT-IR analysis was further carried out to verify the coordination of divalence copper and ligand in compound **1** (Figure 3(b)). Compared with the H<sub>2</sub>dabq ligand, showing strong absorption at 3306 cm<sup>-1</sup> (OH stretching vibration), disappearance of this band in the IR spectra of compound **1** indicated the coordination of ligands with Cu ions [31]. Both the ligand and compound **1** showed prominent bands in the 1500–1600 cm<sup>-1</sup> region that can be assigned as a contribution of C=C and C=O stretching modes [32]. The band at

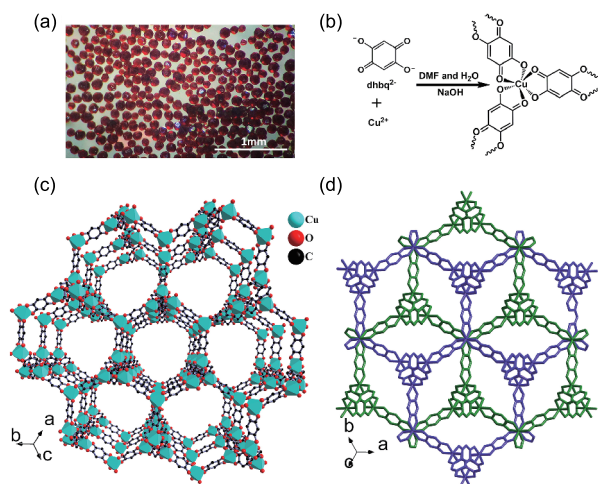


**Figure 2** (a) The optical micrograph of the compound **1** single crystal. (b) Synthetic route.  $\text{NBu}_4\text{I}$  has been omitted for clarity. (c) A larger portion of the crystal structure, showing one of the two  $[\text{Cu}_2(\text{dmbq})_3]^{2-}$  interpenetrated network with (10,3)-a topology that together generate the porous three-dimensional structure. (d) Two independent, enantiomeric, interpenetrating  $[\text{Cu}_2(\text{dmbq})_3]^{2-}$  networks, charge-balancing  $\text{NBu}_4^+$  cations are not depicted for clarity.  $\text{NBu}_4^+$  cations fully occupied the void of framework (color online).

$1638\text{ cm}^{-1}$  of the free ligand, arising from  $\text{C}=\text{O}$  stretching vibration, shifts to lower wavenumber  $1507\text{ cm}^{-1}$  of compound **1**, which is due to the chelation of  $\text{C}=\text{O}$  with metal [33]. We failed to unambiguously assign the other strong band between  $1000$  and  $1500\text{ cm}^{-1}$  to  $\text{C}-\text{C}$ ,  $\text{C}-\text{O}$ , and  $\text{C}-\text{N}$  vibrations [34]. The solid-state UV-Vis-NIR absorbance spectra of the linker molecules and the compound **1** show a broad absorbance extending across the range  $200\text{--}600\text{ nm}^{-1}$ , with absorption edge

$591$  and  $652\text{ nm}^{-1}$ , respectively. A higher wavelength absorbance observed at  $851\text{ nm}^{-1}$  in compound **1** is tentatively assigned to a  $\pi\text{-}\pi^*$  transition, though the feature may also be due to ligand-to-metal charge transfer [35,36]. To study the thermal stability of compound **1**, thermogravimetric measurement was carried out. The result shows well developed platform before  $200\text{ }^\circ\text{C}$ , which illustrate it could be stable up to  $200\text{ }^\circ\text{C}$  without weight loss (Figure 3(d)). The continuous, speedy weight loss upon heating up to  $300\text{ }^\circ\text{C}$  can be attributed to the loss of the counteranions ( $\text{NBu}_4^+$ ) and thus the collapse of whole framework. From the result of elements analysis and thermogravimetric analysis (TG), we can draw a conclusion that the crystal does not contain solvent molecules, and the compound **1** is in fair agreement with the composition of  $(\text{NBu}_4)_2\text{Cu}_2(\text{dmbq})_3$ .

### 3.2 Humidity sensing properties of compound 1

A two-probe method was employed to investigate the conductive properties of compound **1** by a pressed pellet where both faces of the pellet were painted with silver paint. Figure 4 shows a typical semiconductive property of compound **1**. After the ground crystals were immersed into the water for 15 d, it retains the same locations of diffraction peaks, indicating compound **1** crystals show a good water stability (Figure 3(a)). The water stability result suggests that it can be used as chemiresistive humidity sensor. The real-time dynamic response curve displayed in Figure 5(a) shows that the current curve of the humidity sensor presents good response and recovery to a broad range of RH from 30% to 90%. The signal strength is more apparent and larger

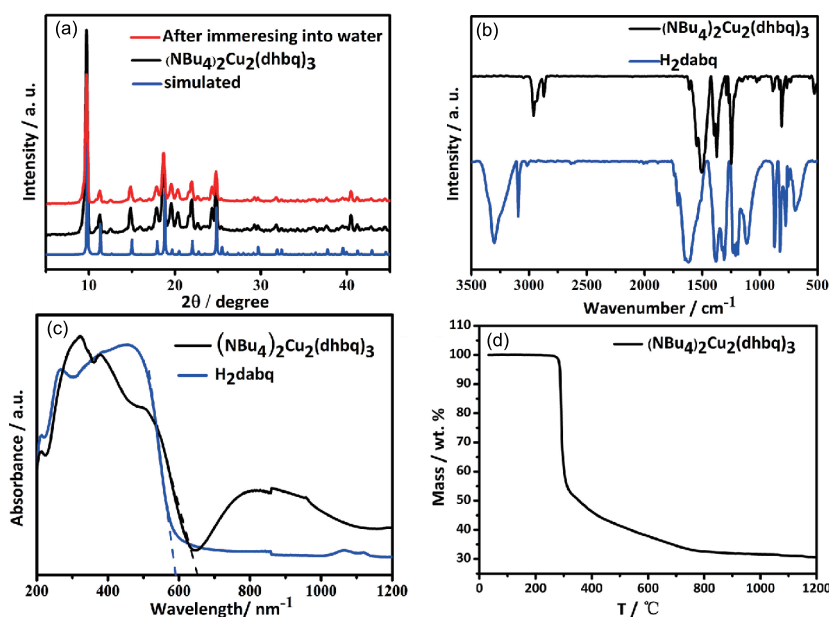


**Figure 3** (a) Powder XRD pattern of compound **1**; (b) FT-IR pattern of compound **1** and  $\text{H}_2\text{dabq}$ ; (c) UV-Vis spectra pattern of compound **1** and the ligand  $\text{H}_2\text{dabq}$ ; (d) TG curve of compound **1** (color online).

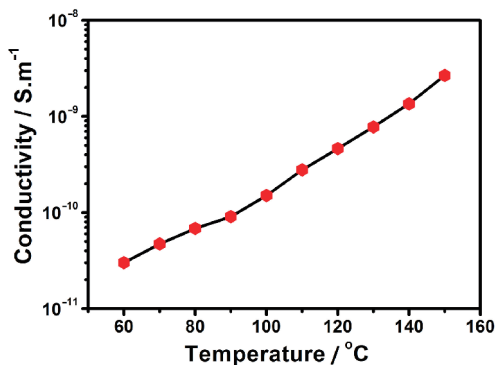


**Figure 4** Temperature dependent conductivity curve of compound **1** (color online).

than noise. When humidity air was mixed in the flow, the electrical current of the sensor promptly increased and then gradually reached a relatively stable value. When reverting to dry air, the current drop faster back to the baseline current with a baseline current at  $10^{-12}$  A. Responses were calculated to reveal the sensing characteristics of the compound **1** toward moisture. The response of the sensor for detecting the humidity in this paper is defined as the ratio of device resistance in dry gas and in humidity gas:

$$R_{\text{response}} = R_{\text{dry}} / R_{\text{humidity}} - 1 = I_{\text{humidity}} / I_{\text{dry}} - 1 \quad (1)$$

The response as a function of RH is presented in Figure 5(b), which exhibited good linearity of humidity response (linear sensitivity) to broad RH range (30%–90% RH). Response reached up to 4 orders of magnitude at 80% RH. From this point of view, compound **1** based humidity sensor is comparable with humidity sensors based on metal

oxides [37,38] and other MOFs [20,22,39] and is better than humidity sensors based on carbon nanotubes [40] and graphene oxide [41–43] (Table 2). The correlation coefficient ( $R^2=0.989$ ) of the linear fitting to the experimental data illustrates good quality of the fit. The repeating dynamic response of compound **1** based sensor to rapid variations in the dry air and 80% RH is shown in Figure 5(c). We tested five cycles under 80% RH. It is observed that the current of the sensor reverts always to the original value, when RH is restored to the former state, indicating that the humidity-sensing process is extremely reversible. The coefficient of variation (CV) is used to describe the effect of humidity on responses which are defined as:

$$CV = R_{\text{SD}} / R_{\text{average}} \times 100\% \quad (2)$$

where  $R_{\text{SD}}$  and  $R_{\text{average}}$  are standard deviation (SD) and average value of response at 80% RH condition, respectively. The humidity sensor showed not only excellent repeatability but also very low value of  $CV=4.8\%$  under 80% RH. The lower CV value means the better anti-interference performance and indicates good repeatability of the sensor [28]. For humidity sensors, reproducibility was evaluated by testing the performance of devices at 80% RH which fabricated by compound **1** synthesized in different batches (Figure S2). The devices showed good repeatability and high responses ( $\sim 10^4$ ). Maybe due to the different size distribution and thickness, slight difference in responses can be observed for different batched of devices, which is acceptable for reproducibility. The sensing performances of humidity sensor have been further studied for its response and recovery time. The response and recovery behaviour is one of the most important characteristics in

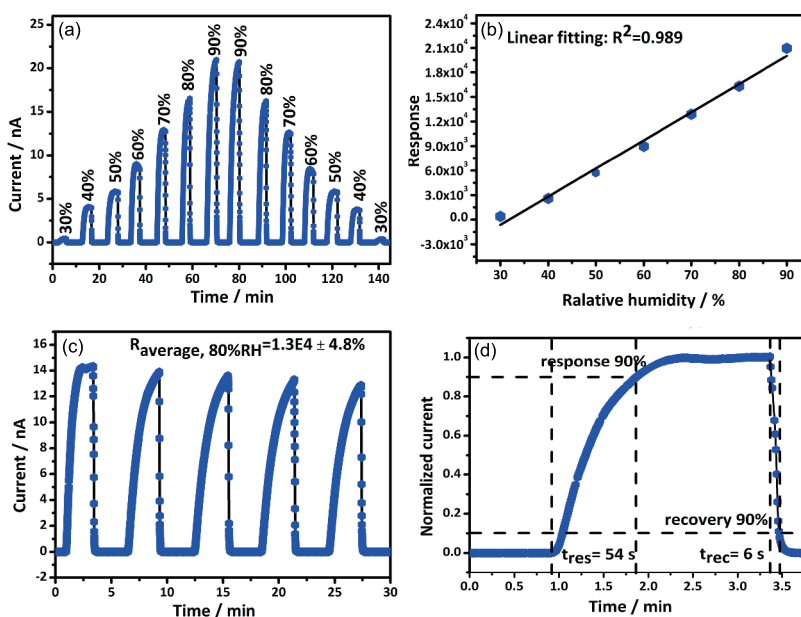


**Figure 5** Compound **1** based humidity sensor. (a) Current response to dry air and different RH (30%–90%) at 25 °C; (b) humidity-dependent responses; (c) the response and recovery under 80% RH for 5 cycles; (d) response and recovery time at 80% RH (color online).

evaluating humidity sensors. We normalized the maximum of current as 1 to estimate the response and recovery properties (Figure 5(d)). Response time is defined as the time taken by the sensor to attain 90% of the final saturation current change in humidity air, while the recovery time is the time for the humidity sensor to recover to 10% of current change above the original current value in air. We calculated response and recovery time of the device at 80% RH. As show in Figure 5(d), it is obvious that recovery speed is faster than response speed. The response time for 80% RH was determined as ca. 54 s, whereas the corresponding recovery time only took 6 s. The adsorption/desorption behaviour of water mainly formed on the sensor surface which makes the H<sub>2</sub>O molecules move through the materials easier, resulting in a rapid recovery speed [26]. Considering the fact that it takes ~39 s to fulfil the quartz chamber when the gas flow was 600 mL min<sup>-1</sup>, the response-recovery results are excellent. In addition, such results are comparable or even better than the previously reported SnO<sub>2</sub> nanowire humidity sensor [38], graphene oxide resistive humidity sensor [42] and conventional capacitive sensors utilizing silicon nanowires [44] and so on (Table 2). Figure 6(a) shows the hysteresis characteristics of the sensor at room temperature. The blue line of the loop represents the changes in current during ad-

sorption process when the RH changes from low value (dry air) to a high value (90%). The red line of the loop represents the changes in current in case of desorption process when the RH changes from a high value to a low value. The adsorption/desorption behaviour based on resistance measurements remains almost constant between 30% and 90% RH, following a narrow hysteresis curve. This narrow hysteresis indicates good reliability of the sensor. In practical applications, hysteretic behaviours are often observed in capacitive humidity sensors and such behaviour is often a serious drawback [18,19]. The testing results presented above indicate that water vapours in air have a strong influence on the conductivity of compound **1**. And such conductivity change resulting from the fluctuation of RH in air is always reversible. All of these characteristics demonstrate its potential application in chemiresistive sensing of moisture.

### 3.3 Humidity sensing mechanism

Water related conduction in sensing materials is known to mainly occur as a surface mechanism [41,45]. And it is believed that the change of resistance along with humidity is closely related with the chemical and subsequently physical absorption of water molecules. The compound **1** possesses

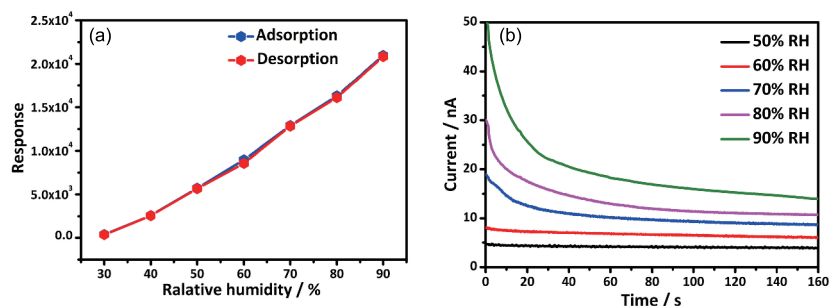


**Figure 6** (a) Humidity hysteresis characteristic of compound **1**; (b) curves of current vs. time of the compound **1** based sensor at various RH obtained by the DC reverse polarity method (color online).

**Table 2** Comparison of various materials-based humidity sensors

Materials	Sensor type	Shape	Detected RH range	Response/recovery time (s)	The highest response	Ref.
Single SnO <sub>2</sub>	DC Resistance	Nanowire	5.0%–85%	120–170/20–60	32	[38]
Graphene oxide	DC Resistance	Flacks	10%–80%	189±49/89±5	~10	[42]
Reduced graphene oxide	DC Resistance	Ultrathin film	4.3%–75.7%	4/10	~0.06	[43]
(NBu <sub>4</sub> ) <sub>2</sub> Cu <sub>2</sub> (dmbq) <sub>3</sub>	DC Resistance	Powder	30%–90%	54/6	2.1×10 <sup>4</sup>	Present work
Cu <sub>3</sub> (BTC) <sub>2</sub>	Capacitance	Thick film	11%–84%	20/20	1.94	[20]
Cu <sub>3</sub> TCP	Capacitance	Pellet	60%–98%	N/A/N/A	42	[22]
CeO <sub>2</sub>	Capacitance/AC resistance	Nanoparticles	11%–98%	10/3	5×10 <sup>3</sup> /2×10 <sup>4</sup>	[37]
NH <sub>2</sub> -MIL-125(Ti)	Capacitance/AC resistance	Powder	11%–95%	45/50	N/A/3.6×10 <sup>4</sup>	[39]
Carbon	Capacitance	Nanotube	11%–97%	45/15	1.5	[40]
Graphene oxide	Capacitance	Thin film	15%–95%	10.5/41	378	[41]
Silicon	Capacitance	Nanowire	11.3%–93%	350/52	1.8	[44]

microporous anion framework but nearly fully encapsulated by a large size counter cations. As a result, the external surfaces of these MOF particles are available for the adsorbed molecules. Thus, its humidity sensing responses mainly depend on outer surfaces of the MOF. There are two possible humidity sensing mechanisms. Most of works including all AC type and some DC type interpreted as contribution of water-induced proton conductivity by a Grotthuss-type mechanism [18,19,41]. However, in some works, the resistance change can be attributed to the reduced potential barrier and the activation energy of the sensing materials caused by water molecules and ionic functional hydroxyl groups adsorbed on grain surfaces, grain boundaries and interfaces between sensing materials and electrodes [46–48].

To probe electronic and ionic contributions to the moisture-induced increase of electrical conduction, instantaneous polarity reversion was applied to the DC circuit [49,50]. We chose 1 V as the operating voltage. The current vs. time at different RH conditions is shown in Figure 6(b). When the DC voltage is put on sensing materials, the current decays exponentially, and the currents stabilize finally at 3 to 4 orders (depending on RH) of magnitude larger than the baseline value. It demonstrated that the total current includes two parts: in the first part, ionic conduction (initial current) dominated the conductivity change, but the ionic current decays exponentially, then electronic conduction (steady state current) began to play the leading role, and the current we tested mainly come from steady current. Such observation implies that, for DC resistive humidity sensor studied in this work, freely transporting ionic/protonic carriers do not seem to dominate the conductivity change. The second interpretation might be the possible sensing mechanism for compound **1** in this work. To obtain a clear DC humidity sensing mechanism, extensive and deep studies on various materials and devices are necessary.

In addition, high responses of the humidity sensor in this work can be attributed to abundant active sites and low charge carrier density of active materials. Firstly, compound **1** has abundant sensing active sites on the surface including metal and –OH groups from the ligand, which enable the extraordinary adsorption of water molecules. Secondly, low charge carrier density of active material can be observed from the temperature dependent on low conductivity curve at humidity free condition in Figure 4. Thus, the conductivity can be greatly affected by the injection of electrons, reduced potential barrier and the activation energy of the sensing materials caused by water molecules and ionic functional hydroxyl groups [46–48]. Both of them contribute to its high humidity sensing responses.

## 4 Conclusions

In conclusion, a semiconductive, water-stable, coordination

polymer material,  $(\text{NBu}_4)_2\text{Cu}_2(\text{dmbq})_3$ , has been prepared and characterized which contained two independent, enantiomeric (10,3)-a networks of opposite chiralities, and showed good water-stable and typical semiconductive behavior. The corresponding DC humidity sensor based on this compound exhibited narrow hysteresis, fast response and recovery, indicating good reliability. Such properties can overcome the existing problems (broad hysteresis and fair response and recovery) of capacitive and AC impedance type humidity sensors. In addition, good linearity of humidity responses to entire RH range (30%–90% RH), together with high response with 4 orders of magnitude at 80% RH, demonstrates its great potential for quantitatively detecting humidity. DC chemiresistive humidity sensor is easy to be integrated with low power consumption standard electronics for real-time monitoring.

**Acknowledgments** This work was supported by the National Natural Science Foundation of China (51402293, 21401193), the Strategic Priority Research Program of Chinese Academy of Sciences (XDB20000000), Key Research Program of Frontier Science, Chinese Academy of Sciences (QYZDB-SSW-SLH023), Scientific Research and Equipment Development Project, Chinese Academy of Sciences (YZ201609), and the Natural Science Foundation of Fujian Province (2016J06006, 2015J01230, 2016J05053, 2017J05034).

**Conflict of interest** The authors declare that they have no conflict of interest.

**Supporting information** The supporting information is available online at <http://chem.scichina.com> and <http://link.springer.com/journal/11426>. The supporting materials are published as submitted, without typesetting or editing. The responsibility for scientific accuracy and content remains entirely with the authors.

- 1 Fennell Jr JF, Liu SF, Azzarelli JM, Weis JG, Rochat S, Mirica KA, Ravnsbaek JB, Swager TM. *Angew Chem Int Ed*, 2016, 55: 1266–1281
- 2 Kaushik A, Kumar R, Arya SK, Nair M, Malhotra BD, Bhansali S. *Chem Rev*, 2015, 115: 4571–4606
- 3 Fine GF, Cavanagh LM, Afonja A, Binions R. *Sensors*, 2010, 10: 5469–5502
- 4 Wisser FM, Grothe J, Kaskel S. *Sensor Actuat B-Chem*, 2016, 223: 166–171
- 5 Wei L, Lu D, Wang J, Wei H, Zhao J, Geng H, Zhang Y. *Sensor Actuat B-Chem*, 2014, 190: 529–534
- 6 Meng FL, Guo Z, Huang XJ. *TrAC Trends Anal Chem*, 2015, 68: 37–47
- 7 Lytvynenko AS, Kolotilov SV. *Theor Exp Chem*, 2016, 52: 197–211
- 8 Zhou HCJ, Kitagawa S. *Chem Soc Rev*, 2014, 43: 5415–5418
- 9 Lin JM, He CT, Liao PQ, Zhou DD, Zhang JP, Chen XM. *Sci China Chem*, 2016, 59: 970–974
- 10 Wang T, Jia Y, Chen Q, Feng R, Tian S, Hu TL, Bu XH. *Sci China Chem*, 2016, 59: 959–964
- 11 Shafiei M, Hoshyargar F, Lipton-Duffin J, Piloto C, Motta N, O'Mullane AP. *J Phys Chem C*, 2015, 119: 22208–22216
- 12 Hoshyargar F, Shafiei M, Piloto C, Motta N, O'Mullane AP. *J Mater Chem C*, 2016, 4: 11173–11179
- 13 Chen EX, Yang H, Zhang J. *Inorg Chem*, 2014, 53: 5411–5413

- 14 Wang F, Wang YT, Yu H, Chen JX, Gao BB, Lang JP. *Inorg Chem*, 2016, 55: 9417–9423
- 15 Campbell MG, Liu SF, Swager TM, Dincă M. *J Am Chem Soc*, 2015, 137: 13780–13783
- 16 Campbell MG, Sheberla D, Liu SF, Swager TM, Dincă M. *Angew Chem Int Ed*, 2015, 54: 4349–4352
- 17 Smith MK, Jensen KE, Pivak PA, Mirica KA. *Chem Mater*, 2016, 28: 5264–5268
- 18 Lee CY, Lee GB. *Sen Lett*, 2005, 3: 1–15
- 19 Farahani H, Wagiran R, Hamidon MN. *Sensors*, 2014, 14: 7881–7939
- 20 Liu J, Sun F, Zhang F, Wang Z, Zhang R, Wang C, Qiu S. *J Mater Chem*, 2011, 21: 3775–3778
- 21 Feng J, Kang X, Zuo Q, Yuan C, Wang W, Zhao Y, Zhu L, Lu H, Chen J. *Sensors*, 2016, 16: 314
- 22 Tian M, Fu ZH, Nath B, Yao MS. *RSC Adv*, 2016, 6: 88991–88995
- 23 Achmann S, Hagen G, Kita J, Malkowsky IM, Kiener C, Moos R. *Sensors*, 2009, 9: 1574–1589
- 24 Zhang J, Sun L, Chen C, Liu M, Dong W, Guo W, Ruan S. *J Alloys Compd*, 2017, 695: 520–525
- 25 Li T, Li L, Sun H, Xu Y, Wang X, Luo H, Liu Z, Zhang T. *Adv Sci*, 2017, 4: 1600404
- 26 Wang L, He Y, Hu J, Qi Q, Zhang T. *Sensor Actuat B-Chem*, 2011, 153: 460–464
- 27 Sheldrick GM. *Acta Crystlogr A Found Adv*, 2015, 71: 3–8
- 28 Yao MS, Tang WX, Wang GE, Nath B, Xu G. *Adv Mater*, 2016, 28: 5229–5234
- 29 Abrahams BF, Hudson TA, McCormick LJ, Robson R. *Cryst Growth Des*, 2011, 11: 2717–2720
- 30 Chui SSY, Lo SMF, Charmant JPH, Orpen AG, Williams ID. *Science*, 1999, 283: 1148–1150
- 31 Akai N, Kudoh S, Takayanagi M, Nakata M. *J Phys Chem A*, 2002, 106: 11029–11033
- 32 de Oliveira LFC, Edwards HGM, Velozo ES, Nesbitt M. *Vib Spectrosc*, 2002, 28: 243–249
- 33 Mostafa SI. *Trans Metal Chem*, 1999, 24: 306–310
- 34 Socrates G. *Infrared and Raman Characteristic Group Frequencies: Tables and Charts*. Chichester: John Wiley & Sons, 2004
- 35 Halis S, Inge AK, Dehning N, Weyrich T, Reinsch H, Stock N. *Inorg Chem*, 2016, 55: 7425–7431
- 36 Darago LE, Aubrey ML, Yu CJ, Gonzalez MI, Long JR. *J Am Chem Soc*, 2015, 137: 15703–15711
- 37 Xie W, Liu B, Xiao S, Li H, Wang Y, Cai D, Wang D, Wang L, Liu Y, Li Q, Wang T. *Sensor Actuat B-Chem*, 2015, 215: 125–132
- 38 Kuang Q, Lao C, Wang ZL, Xie Z, Zheng L. *J Am Chem Soc*, 2007, 129: 6070–6071
- 39 Zhang Y, Chen Y, Zhang Y, Cong H, Fu B, Wen S, Ruan S. *J Nanopart Res*, 2013, 15: 2014
- 40 Chen WP, Zhao ZG, Liu XW, Zhang ZX, Suo CG. *Sensors*, 2009, 9: 7431–7444
- 41 Bi H, Yin K, Xie X, Ji J, Wan S, Sun L, Terrones M, Dresselhaus MS. *Sci Rep*, 2013, 3: 2714
- 42 De Luca A, Santra S, Ghosh R, Ali SZ, Gardner JW, Guha PK, Udrea F. *Nanoscale*, 2016, 8: 4565–4572
- 43 Wang X, Xiong Z, Liu Z, Zhang T. *Adv Mater*, 2015, 27: 1370–1375
- 44 Chen X, Zhang J, Wang Z, Yan Q, Hui S. *Sensor Actuat B-Chem*, 2011, 156: 631–636
- 45 Ahmadipour M, Ain MF, Ahmad ZA. *Measurement*, 2016, 94: 902–908
- 46 Yeh YC, Tseng TY. *J Mater Sci*, 1989, 24: 2739–2745
- 47 Zhang T, He Y, Wang R, Geng W, Wang L, Niu L, Li X. *Sensor Actuat B-Chem*, 2008, 131: 687–691
- 48 Sun C, Karthik KRG, Pramana SS, Wong LH, Zhang J, Yizhong H, Sow CH, Mathews N, Mhaisalkar SG. *J Mater Chem C*, 2014, 2: 940–945
- 49 Jiang K, Fei T, Jiang F, Wang G, Zhang T. *Sensor Actuat B-Chem*, 2014, 192: 658–663
- 50 Jiang K, Zhao H, Fei T, Dou H, Zhang T. *Sensor Actuat B-Chem*, 2016, 222: 440–446